

Copyright © 1987, by the author(s).
All rights reserved.

Permission to make digital or hard copies of all or part of this work for personal or classroom use is granted without fee provided that copies are not made or distributed for profit or commercial advantage and that copies bear this notice and the full citation on the first page. To copy otherwise, to republish, to post on servers or to redistribute to lists, requires prior specific permission.

**NONLINEAR DYNAMICS OF A DIGITAL PHASE
LOCKED LOOP**

by

G. M. Bernstein, M. A. Lieberman, and A. J. Lichtenberg

Memorandum No. UCB/ERL M87/59

25 August 1987

ELECTRONICS RESEARCH LABORATORY

College of Engineering
University of California, Berkeley
94720

Nonlinear Dynamics of a Digital Phase Locked Loop *

G. M. Bernstein, M. A. Lieberman and A. J. Lichtenberg

Department of Electrical Engineering and Computer Sciences,
and the Electronics Research Laboratory
University of California, Berkeley CA 94720

Abstract

A second order digital phase locked loop may exhibit unusual behavior for some parameters due to a fractal boundary between the basin of attraction of the *locked* fixed point and the attracting basins of coexisting periodic orbits. The usual optimization criterion of the loop parameters using linearized analysis is insufficient, due to coexisting periodic orbits. We present a new optimization procedure based upon numerical bifurcation studies. We obtain numerical estimates of average lock time which can be approximated analytically using the rate of contraction of the phase space in a neighborhood of the fixed point, together with the size of the phase space that is regular for the underlying Hamiltonian approximation.

* Research sponsored by National Science Foundation Grant ECS-8517364 and by Office of Naval Research Contract N00014-84-K-0367.

1. Introduction

The nonuniformly sampling digital phase locked loop (DPLL) has been frequently studied over the years [1, 2, 3]. In a previous paper [3] the nonlinear equations describing the DPLL were linearized about the locked state and the loop parameters were optimized for the fastest linear convergence to that state. Using these parameters, not all of the initial conditions in the phase space were seen to converge; that is, infinite cycle slipping was observed. Moreover, the boundary between those initial conditions that converged and those that did not converge was not well defined; that is, the system seemed very sensitive to initial conditions.

In this paper we will show that this phenomena is due to a period-4 orbit that coexists with the locked fixed point, and that the observed sensitivity to initial conditions is due to the fractal structure of the boundary between the basins of attraction for the period-4 orbit and the fixed point. In addition, we show using numerically computed bifurcation diagrams that one can choose parameters such that almost all initial conditions will converge to the locked fixed point. Using bifurcation theory along with numerical simulations we can choose parameter values that give the maximum lock range. We examine the convergence statistics for the DPLL using a theory developed to determine the convergence rate for weakly dissipative mappings [11]. We estimate the convergence rates of the DPLL and compare with the numerical results.

The block diagram of the DPLL is shown in Fig. 1. The period of the digitally controlled oscillator (DCO), $T_k \equiv t_k - t_{k-1}$, is controlled by the output, y_k , of the digital filter as follows:

$$T_k = T - y_{k-1} \quad \text{with} \quad T = \frac{2\pi m}{\omega_0}, \quad (1)$$

where ω_0 is the nominal operating frequency of the DPLL and m is a positive integer. The input signal is $s(t) = A \sin(\omega_1 t + \theta_0)$. The z-transform of the of the output of the digital filter is:

$$Y(z) = \left(G_1 + \frac{G_2}{1 - z^{-1}} \right) S(z), \quad (2)$$

where $S(z)$ is the z-transform of $s(t)$. We define the phase error, ϕ_k , as follows:

$$\phi_k \equiv \omega_1 t_k + \theta_0 - \omega_0 \sum_{i=0}^{k-1} y_i. \quad (3)$$

The scalar second order equation describing the system can be written:

$$\phi_{n+1} - 2\phi_n + \phi_{n-1} = -\omega_1 A(G_1 + G_2) \sin \phi_n + \omega_1 G_1 A \sin \phi_{n-1}. \quad (4)$$

Defining

$$I_n = \phi_n - \phi_{n-1}, \quad (5)$$

$$k' = \omega_1 G_1 A, \quad (6a)$$

and

$$r = \left(1 + \frac{G_2}{G_1}\right), \quad (6b)$$

where we assume $A > 0$, $G_1 > 0$ and $G_2 > 0$, then equation (4) can be written:

$$I_{n+1} = I_n - rk' \sin \phi_n + k' \sin(\phi_n - I_n), \quad (7a)$$

$$\phi_{n+1} = \phi_n + I_{n+1}, \quad (7b)$$

and substituting for I_{n+1} we have

$$\phi_{n+1} = \phi_n + I_n - rk' \sin \phi_n + k' \sin(\phi_n - I_n). \quad (7c)$$

The above equations exhibit a circular symmetry in ϕ_n and I_n , that is, if we change ϕ_n and/or I_n by a multiple of 2π then I_{n+1} and ϕ_{n+1} will stay the same modulo- 2π . We can therefore restrict ϕ_n and I_n to $[0, 2\pi]$, where we identify 0 and 2π , i.e., $(I_n, \phi_n) \in T^2$, the torus.

2. Basins of Attraction

In reference [3] the stability of the fixed point, $I = 0$, $\phi = 0$, of equation (7) was studied using linearization.

Denoting the mapping in equation (7) as $(I_{n+1}, \phi_{n+1}) = f(I_n, \phi_n)$ the jacobian of the mapping is:

$$Df(I, \phi) = \begin{pmatrix} 1 - k' \cos(\phi - I) & -rk' \cos \phi + k' \cos(\phi - I) \\ 1 - k' \cos(\phi - I) & 1 - rk' \cos \phi + k' \cos(\phi - I) \end{pmatrix}. \quad (8)$$

At $(I, \phi) = (0, 0)$, we obtain

$$Df(0, 0) = \begin{pmatrix} 1 - k' & -rk' + k' \\ 1 - k' & 1 - rk' + k' \end{pmatrix}. \quad (9)$$

Osborne chose the parameters $k' = 1$ and $r = 2$, since for these parameters three elements of the jacobian are zero and the spectral radius, the maximum of the magnitude of all the eigenvalues, is zero. These parameters give optimally fast convergence near the fixed point $(0, 0)$.

Although reference [3] pointed out the existence of a number of period-2 orbits, none of which are stable for the above k' and r , a stable period-4 orbit exists, with $\phi_1 = 2.9556$, $\phi_2 = 5.4536$, $\phi_3 = 3.3265$ and $\phi_4 = 0.8296$, which gives rise to the *infinite cycle slipping* observed. To understand the observed sensitivity

to small changes in initial conditions, that is, two initial conditions close to each other may lead to different asymptotic behavior, we calculate the basins of attraction of the fixed point at $(0,0)$ and the period-4 orbit. The basin of attraction of a fixed point or periodic orbit is just the set of all initial conditions that eventually converge to the fixed point or periodic orbit. We can easily calculate approximate basins of attraction by iterating a grid of initial conditions in the I - ϕ phase space with the mapping $f(I, \phi)$ and classifying them according to whether they converge to the fixed point or the period-4 orbit.

In Fig. 2a we show in black the initial conditions that converge to the period-4 orbit within 200 iterations. Except for small neighborhoods surrounding the points of the unstable period-2 orbit, $(I_1, \phi_1) = (\pi, \pi)$, $(I_2, \phi_2) = (\pi, 0)$, all other grid points converge to the fixed point $(I, \phi) = (0, 0)$ modulo- 2π , which corresponds to the four corners of Fig. 2a. To see if the boundary between the two basins of attraction is fractal we enlarge the boxed section of Fig. 2a., which we show in Fig. 2b., and in turn enlarge the boxed section of Fig. 2b which we show in Fig. 2c.

The continuous interleaving of the basins on different length scales suggests the fractal nature of the boundary. Fractal basin boundaries have been observed in a number of nonlinear systems including continuous time systems [4, 5], notably in the differential equations describing the forced damped pendulum.

3. Operating Parameters

Our main tool for evaluating parameter values for the DPLL is from numerically calculated bifurcation diagrams, (see Fig. 3). Bifurcation diagrams were first used to study the changes in the structure of fixed points and periodic orbits of one-dimensional maps with respect to changes in a parameter [6]. They are also useful in higher dimensions if care is taken in their interpretation. Along the horizontal axis of the bifurcation diagram a parameter of the system is varied, k' in Fig. 3, while vertically we plot successive iterates of a state variable for the system; I_n in Fig. 3a, ϕ_n in Fig. 3b. For each value of the system parameter we first select a set of initial conditions; in Fig. 3 we use a line of 20 points between $(0, 0)$ and $(2\pi, 2\pi)$ for every value of k' . Next we iterate that set of initial conditions for n_{out} preliminary iterations to eliminate most of the *transient* behavior. Finally, we plot n_{its} succeeding iterations of the state variable of interest.

When interpreting the bifurcation diagrams for the DPLL the following observations are useful. (1) The equations were defined on a torus, hence 0 and 2π are the same point, for both I and ϕ . For example, in Fig. 3a and 3b at $k' = 1.2$ we see I_n and ϕ_n taking on the value 0 and 2π which are the same on the torus, and hence the locked state. (2) A set of initial conditions is used; hence we may see more than one periodic

orbit or fixed point at a system parameter value. This is evident for example in Fig. 3a when $k' = 0.76$. From the iterates in the phase space, (I, ϕ) , we find two distinct period-3 orbits, a period-2 orbit and a fixed point, all coexisting for the same parameter value. (3) Since we observe only one state variable of the system at a time, one state variable may be changing while another is constant. For example, the period-2 point $(\pi, 0)$, (π, π) could be misinterpreted as a fixed point from Fig. 3a, alone.

The bifurcation diagrams of Fig. 3 indicate that, for the *linear optimal* parameters $k' = 1.0$, $r = 2.0$, we have both a period-4 orbit and the fixed point of the locked state $(0, 0)$. This is clearly undesirable if we want our loop to lock under most initial conditions. However, for $k' = 1.2$ we see only the $(0, 0)$ fixed point. Following a 100×100 grid of initial points for this k' , all grid points converged within 100 iterations to the fixed point $(0, 0)$.

When selecting operating parameters r and k' , no other stable fixed points or periodic orbits besides the locked $(0, 0)$ fixed point should exist; or if they do exist their basins of attraction should be small enough to be insignificant for practical purposes. Furthermore, we maximize the lock range in k' , that is, we maximize the percentage by which we can change k' (proportional to the driving frequency) and still have the loop lock for all initial conditions. The important issue of average time to lock is addressed in the next section.

We reduce the number of r and k' values to be considered by determining the stability regions of the fixed point at $(0, 0)$ and the period-2 orbit at $(I_1, \phi_1) = (\pi, 0)$, $(I_2, \phi_2) = (\pi, \pi)$. Linearizing the mapping $f(I, \phi)$ about the locked fixed point at $(0, 0)$ the eigenvalues of (9), indicate that it becomes unstable, via a period doubling bifurcation, for

$$k' > \frac{4}{1+r}. \quad (10)$$

This is seen in Fig. 3, where $k' = 4/3$. Linearizing the mapping $f(f(I, \phi))$ about $(\pi, 0)$ using the chain rule and equation (8), we find that the period-2 orbit, which is stable for small k' , becomes unstable, via a period doubling bifurcation, for

$$k' > \frac{2}{\sqrt{1+r^2}}. \quad (11)$$

We can see that the period-2 orbit bifurcates to a period-4 orbit in the bifurcation diagram of Fig. 3 at $k' = 2/\sqrt{5}$. From the above we restrict k' to the range:

$$\frac{2}{\sqrt{1+r^2}} < k' < \frac{4}{1+r}. \quad (12)$$

To further restrict the possible r and k' values we resort to numerical methods. In Figs. 4(a)-(c) we show bifurcation diagrams for $r = 2, 4, 6$ respectively, with k' running through the range specified by the

inequalities (12). For low k' values, i.e., towards the left side of the diagrams, we see the presence of a period-4 orbit. This period-4 orbit becomes unstable for larger k' values via a Hopf bifurcation [7, 8], i.e., if we linearize about the period-4 orbit the eigenvalues are complex when they cross the unit circle. In Fig. 4(a) we also have a period-12 orbit appearing; however further studies have shown that this orbit becomes unstable via a Hopf bifurcation before the period-4 orbit goes unstable. The equations giving this period-4 orbit can be reduced to:

$$2\phi_2 + k' \sin \phi_1 - k'r \sin \phi_2 = 4\pi \quad (13a)$$

$$2\phi_1 - k'r \sin \phi_1 - k' \sin \phi_2 = 2\pi \quad (13b)$$

$$\phi_1 + \phi_3 = 2\pi \quad (13c)$$

$$\phi_2 + \phi_4 = 2\pi \quad (13d)$$

Since, the eigenvalues are complex when they go unstable their magnitude squared is given by the determinant of the jacobian of the system linearized about the period-4 orbit:

$$\det(Df_{\text{period-4}}) = (1 - k' \cos \phi_1)^2 (1 - k' \cos \phi_2)^2 \quad (14)$$

To find where in k' this period-4 orbit becomes unstable for a given r we set equation (14) equal to one and using equations (13a) and (13b) we solve for ϕ_1 , ϕ_2 and k' . We show this k' value versus r as the lowest curve in Fig. 5, and denote this orbit as the period-4A orbit.

For larger r values, as shown on the right hand side of Fig. 4(c), we see the birth of another period-4 orbit which we denote by period-4B. The period-4B orbit is born via a saddle-node bifurcation; i.e., the eigenvalues of the linearized system are real and one of them equals +1 when the orbit is born. Since the eigenvalue equation is far more complicated than the determinant equation (14), we used a simple boundary search technique to find k' as a function of r where the period-4B orbit is born. The upper solid line in Fig. 5 shows the dependence of k' on r for the birth of this orbit.

The dashed line in Fig. 5 shows where the locked fixed point goes unstable. The shaded area in Fig. 5 indicates the desired region of loop operation. Using the results shown in Fig. 5 we can pick k' and r to maximize the lock range, $LR \equiv \Delta k'/k$, where $\Delta k'$ is the maximum change in k' that can occur and still allow convergence to the locked state. Our calculations show that this occurs for $r = 4.25$ and $k' = 0.64$ with a lock range of approximately 19%. The data of Fig. 5 must be used with some caution. First, the period-4A orbit goes unstable via a Hopf bifurcation [7, 8], which means that for k' values close to the lower

solid line in Fig. 5, almost-periodic solutions usually exist. For example, from the numerical calculations at $r = 2.0$, the period-4A orbit goes unstable at $k' = 1.0830$. The Hopf bifurcation theorem predicts the existence of an almost-periodic orbit near the unstable period-4A orbit. This almost-periodic orbit is seen in Fig. 6, where $r = 2.0$ and $k' = 1.0850$. Hence the lower bound on k' in Fig. 5 is not an exact bound. The same can be said for the upper bound in Fig. 5, since operating too close to it can have deleterious effects on the rate of convergence.

4. Rates of Convergence

In this section we show that the average convergence rate is slower than the convergence rate predicted by linearizing the system near the locked state. To do this we calculate the convergence statistics for a grid of initial conditions as a function of the number of iterations of the system. We compare our results with the linear theory and give a method of estimating the convergence rate outside the region of validity of the linear theory.

To compute the convergence statistics for the DPLL on the torus we need a computationally convenient metric. We choose the following metric for the circle $[0, 2\pi]$, where 0 and 2π are identified:

$$d_C(x, y) = \min(|x - y|, 2\pi - |x - y|), \quad x, y \in [0, 2\pi] \quad (15)$$

and then extended it to the torus in the standard way:

$$d((I_1, \phi_1), (I_2, \phi_2)) = d_C(I_1, I_2) + d_C(\phi_1, \phi_2) \quad (16)$$

With this metric we computed the RMS statistics as follows:

$$RMS(n) = \sqrt{\frac{1}{n_{pts}} \sum_{i=1}^{n_{pts}} d((I_{n,i}, \phi_{n,i}), (0, 0))^2} \quad (17)$$

where n_{pts} is the number of points in the grid of initial conditions, and n is the iteration count. Since (17) tends to be exponential with n , it is more informative to plot the logarithm of (17), rather than (17) itself.

In Figs. 7(a)-(d) we show plots of $\ln RMS(n)$, where $r = 4.0$, for k' running from the lower to upper bounds as set by Fig. 5. The $\ln RMS(n)$ curves of Figs. 7(a) and (d) indicate markedly inferior convergence characteristics. For Fig. 7(a) with a k' near the lower bound shown in Fig. 5, this is due to the presence of almost periodic orbits. For Fig. 7(d) with k' near the upper bound shown in Fig. 5, Fig. 7(d), this is due to the locked fixed point being on the verge of instability. Figs. 7(b)-(c) show $\ln RMS(n)$ curves that exhibit a

distinctive piecewise linear character, first the curves appear approximately linear with a given slope, then a breakpoint is reached and the curve once again appears linear with a steeper slope. We expect, once most of the points get fairly close to the locked state at $(0,0)$, that the convergence will be as predicted by the linear theory; i.e., the slope α of the $\ln RMS(n)$ curve for large n , will be related to the eigenvalues, λ_1 and λ_2 of the linearized system as follows:

$$\alpha = \ln(\max(|\lambda_1|, |\lambda_2|)) \quad (18)$$

In the Table I we have used α_1 , α_2 and α_L to denote the slopes of the $\ln RMS(n)$ curves obtained from the approximate slope of the first line segment of the computed $\ln RMS(n)$ plots, the approximate slope of the second line segment in the computed $\ln RMS(n)$ plots, and from the linear theory, respectively. From Table I we see that the slope α_2 of the second line segment is in very good agreement with the convergence rate α_L predicted by the linear theory. In addition we notice that the slope α_1 of the first line segment, is almost an order of magnitude smaller than that of $\alpha_2 \approx \alpha_L$. The same behavior is observed for other r values; hence for most initial conditions the linear theory is inadequate in predicting the overall rates of convergence to the locked state of the DPLL.

The observed $\ln(RMS(n))$ plots indicate transiently chaotic behavior. Transient chaos often appears in nonlinear dissipative dynamical systems as an initial behavior of the motion before the system finally settles into a periodic or almost-periodic steady state. Since this is not a precise definition, usually some criteria such as the presence of Smale Horseshoes or a saddle point having a transverse intersection of its stable and unstable manifolds is used. See reference [8] for more information, and for an example of the dynamics of a bouncing ball, using a map similar to the map for the DPLL. In reference [9], Żóltowski establishes rigorously the existence of transient chaos in the DPLL, however no estimate of the rate of convergence is made.

To obtain estimates of the rate of convergence to the locked state of the DPLL outside the region of validity of the linear theory we will use some ideas developed in the theory of nonlinear mappings. The main idea we use from lossless (Hamiltonian) dynamics is the existence of boundaries in state space between the areas where chaotic and regular motion appear. See Lichtenberg and Lieberman [10] for more details. Our approach is similar to that used in reference [11], where the Fermi map was studied as a lossless system, which exhibits chaotic and regular motion, perturbed by a dissipative term.

The determinant of the jacobian of the map describing the DPLL, equation (8), gives a local rate of expansion or contraction of an area. The determinant is:

$$\det(Df) = 1 - k' \cos(\phi - I). \quad (19)$$

Depending on k' , ϕ and I we may see local expansion, contraction or preservation of areas. In a lossless (Hamiltonian) system, areas (measures) are preserved; hence, the determinant of the jacobian is one over the entire state space. Expanding the term $k' \sin(\phi_n - I_n)$ from equations (7a) and (7b) in I , then the lowest order part, independent of I , may be combined with the remaining mapping to give an area preserving (Hamiltonian) mapping

$$I_{n+1} = I_n - (r-1)k' \sin \phi_n \quad (20a)$$

$$\phi_{n+1} = \phi_n + I_n - (r-1)k' \sin \phi_n \quad (20b)$$

The above mapping has been extensively studied [10] and is known as the *standard map*. The *standard map* is usually written in the form:

$$I_{n+1} = I_n - K \sin \phi_n \quad (21a)$$

$$\phi_{n+1} = \phi_n + I_{n+1} \quad (21b)$$

where $K = k'(r-1)$ is known as the *stochasticity* parameter. In Figs. 8(a)-(d) we show successive plots of the trajectories of the *standard map* for values of the *stochasticity* parameter K running from 1.60 to 2.40, which spans the *good* values of k' at $r = 4$. To obtain these pictures we started with a 25×25 grid of initial conditions and plotted 100 successive iterations of this initial grid. One can clearly see distinct regions of regular and stochastic motion. By stochastic motion we mean that trajectories of this deterministic system undergo motion that appears random. In the terminology of [10] we call the regions of predominantly regular motion *regular islands* and consider them as surrounded by a *stochastic sea* in which the motion is predominantly chaotic.

To obtain an estimate of the decay rate of the transient chaos, we make a probabilistic model of the system dynamics. We assume that when the dissipation term is restored to the system the island centers become attracting fixed points and the regions of stochastic motion become regions of transient chaos. Furthermore, the regular islands become attracting regions where convergence to fixed points is at approximately the linearly predicted rate. This has been confirmed by calculating the RMS statistics for this region alone. We assume that the distribution of trajectory points in the transient chaos region is uniform. This has been verified on the average by calculating the cumulative averaged distribution functions for I and ϕ . For our estimate we assume that with each iteration the attracting region will "capture" a number of initial conditions from the transient chaos region proportional to its net contraction. Let \bar{A} , A and c denote the area of the regular island, the area of the entire phase space and the fractional contraction per iteration

of the attracting region, respectively. If \bar{A} contracts by an amount c then we assume that the attracting region captures $1 - (1 - c)\bar{A}/(A - \bar{A})$ of the initial conditions from the transient chaos region. If we ignore the phase space of the attracting region \bar{A} we get the following RMS statistics based on this model:

$$\ln RMS(n) = \frac{1}{2} \ln \left(\frac{7\pi^2}{6} \right) + \frac{n}{2} \ln \left(1 - \frac{(1 - c)\bar{A}}{A - \bar{A}} \right) \quad (22)$$

The local rate of contraction is given by equation (19). The lowest order estimate of the contraction rate c of the entire regular area surrounding the fixed point $(0, 0)$ is the contraction rate at the origin $c = |1 - k'|$. From [11] the area \bar{A} of the regular regions as a function of the *stochasticity* parameter K can be approximated by $\bar{A} = 2\pi^2 K^{-1.3}$, where the total area A of the state space is $4\pi^2$. Combining these, we obtain

$$\alpha' = \frac{1}{2} \ln \left(1 - (1 - |1 - k'|) \frac{K^{-1.3}}{2 - K^{-1.3}} \right) \quad (23)$$

as our estimate of the convergence rate. In Table II we compare the measured convergence rate α_1 and the estimated convergence rate α' for various k' and r values. From Table II we see reasonable agreement between α' and α_1 .

6. Conclusion

In this paper we have shown that linear analysis of the DPLL is inadequate for optimizing operating parameters. We found, that the occasional lack of locking which depended sensitively on initial conditions, previously reported for the DPLL, was due to the existence of a fractal boundary between the basins of attraction of the locked fixed point and a period-4 orbit that existed simultaneously with the fixed point. The bifurcation diagrams indicated parameter regions for which the period-4 orbit did not exist, and for which all tested initial conditions converged to the period-1 fixed point (locked state). It was shown numerically that for a broad set of initial conditions, the convergence to the fixed point proceeded in two steps. In the initial time period, governed by transient chaos, the convergence is slow. This was followed by a rapid rate governed essentially by the eigenvalues of the DPLL linearized about the fixed point. The initial slower convergence was estimated, analytically, using a method developed previously for weakly dissipative mappings.

7. References

- [1] W. C. Lindsey and C. M. Chie, "A Survey of Digital Phase-Locked Loops", *Proceedings of the IEEE*, April, 1981.
- [2] H. C. Osbourne, "Stability Analysis of an Nth Power Digital Phase-Locked Loop — Part I: First-Order DPLL", *IEEE Transactions on Communications*, August, 1980.
- [3] H. C. Osbourne, "Stability Analysis of an Nth Power Digital Phase-Locked Loop — Part II: Second- and third- order DPLL's", *IEEE Transactions on Communications*, August, 1980.
- [4] Steven W. McDonald, Celso Grebogi, Edward Ott and James A. Yorke, "Structure and Crises of Fractal Basin Boundaries", *Physics Letters*, Vol. 107, No. 2, January 1985.
- [5] Celso Grebogi, Edward Ott and James A. Yorke, "Metamorphoses of Basin Boundaries in Nonlinear Dynamical Systems", *Physical Review Letters*, Vol. 56, No. 10, March 1986
- [6] P. Collet and J.-P. Eckmann, *Iterated Maps on the Interval as Dynamical Systems*, 1980, Birkhäuser, Boston.
- [7] G. Iooss, *Bifurcation of Maps and Applications*, North-Holland Publishing Company, 1979.
- [8] John Guckenheimer and Philip Holmes, *Nonlinear Oscillations, Dynamical Systems, and Bifurcations of Vector Fields*, Springer-Verlag, 1983.
- [9] Mariusz Żółtowski, "Chaotic Transient Hang Up Phenomenon and N:1 Phase Entrainment in Discrete time Phase-Locked Loop of Second Order", *To appear in: Proc. ECCTD-87, Paris, Sept. 1987.*
- [10] A. J. Lichtenberg and M. A. Lieberman, *Regular and Stochastic Motion*, Springer-Verlag, 1983.
- [11] Kwok Yeung Tsang and M. A. Lieberman, "Transient Chaotic Distributions in Dissipative Systems", *Physica 21D*, (1986), 401-414.

k'	α_1	α_2	α_L
0.6143	-0.063	-0.50	-0.48
0.6514	-0.071	-0.56	-0.53
0.6883	-0.074	-0.60	-0.58
0.7257	-0.089	-0.68	-0.65
0.7629	-0.091	-0.32	-0.32

Table I

Slopes of the $\ln(RMS(n))$. α_1 and α_2 are the slopes taken from the plots assuming a piecewise linear characteristic. α_L is the slope as predicted by the linear theory. $r = 4.0$.

r	k'	K	α_1	α'
3.5	0.730	1.83	-0.071	-0.122
3.5	0.769	1.92	-0.074	-0.117
3.5	0.809	2.02	-0.095	-0.113
3.5	0.849	2.12	-0.100	-0.109
4.0	0.614	1.84	-0.063	-0.099
4.0	0.651	1.95	-0.071	-0.095
4.0	0.688	2.06	-0.074	-0.091
4.0	0.726	2.18	-0.089	-0.088
4.0	0.763	2.29	-0.091	-0.085
4.5	0.577	2.02	-0.065	-0.078
4.5	0.613	2.15	-0.069	-0.075
4.5	0.649	2.27	-0.074	-0.073
4.5	0.664	2.32	-0.087	-0.072

Table II

Transient chaos decay rates for various r and k' values. α_1 is the measured rate from the $\ln(RMS)$ plots. α' is the estimated decay rate.

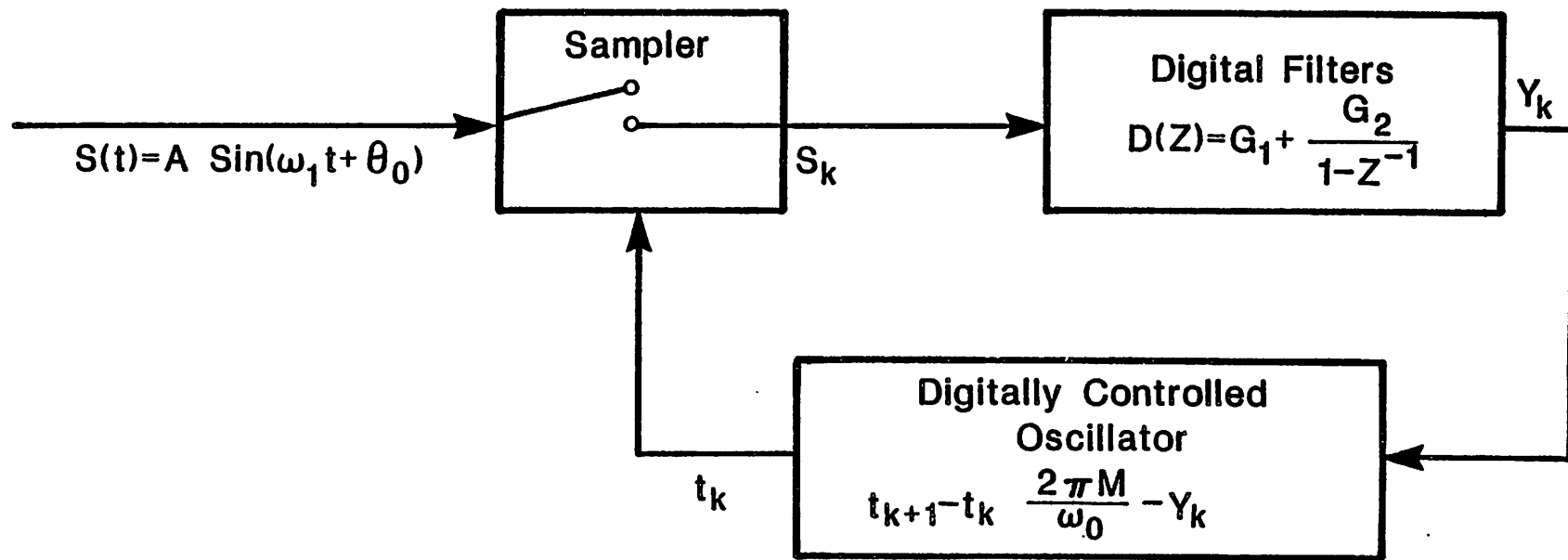


Fig. 1. Block diagram of the nonuniformly sampling DPLL.

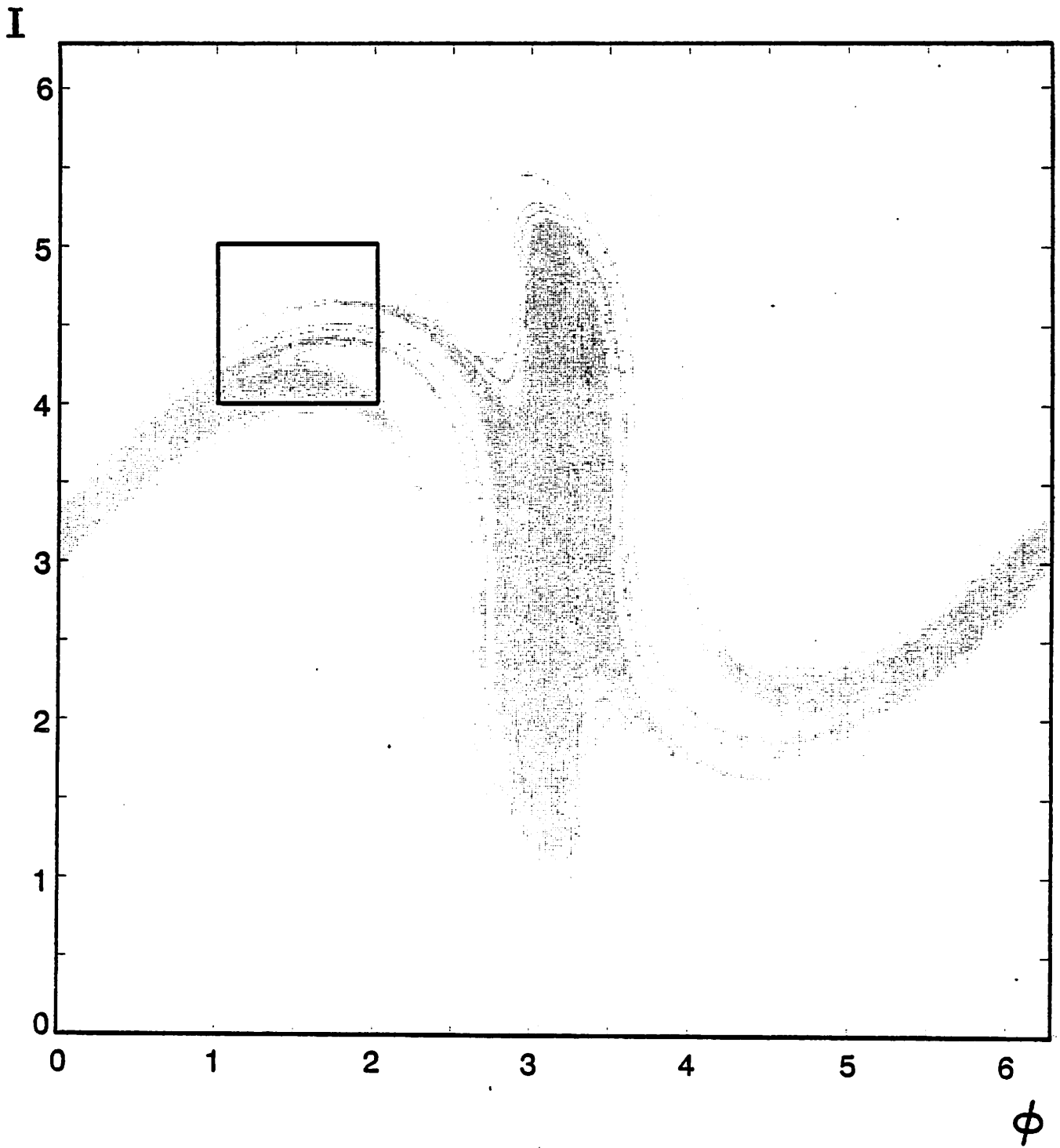


Fig. 2(a). Basin of attraction of the period-4 orbit. Points converging to the period-4 orbit are shown in black. Entire phase space.

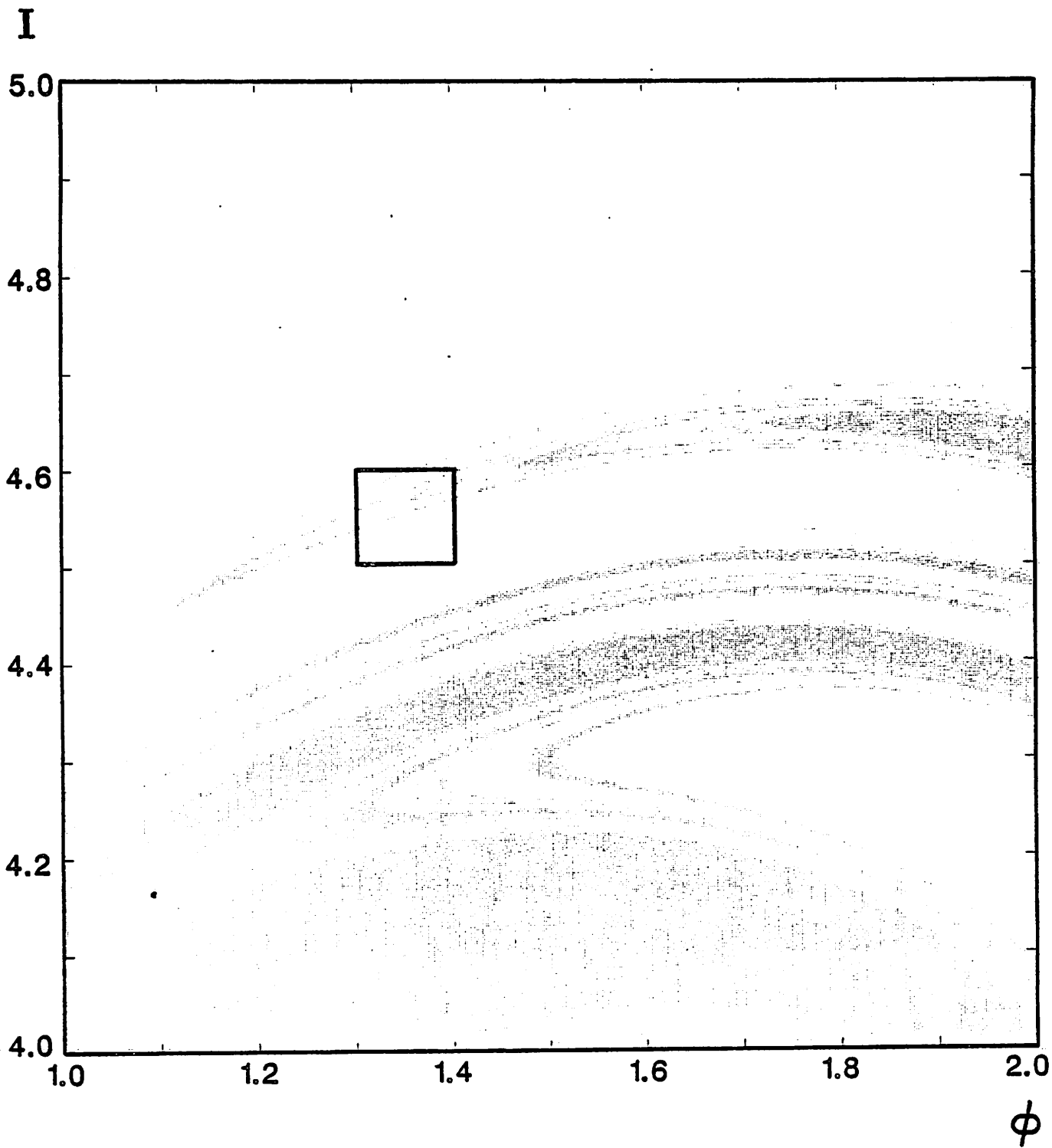


Fig. 2(b). Basin of attraction of the period-4 orbit. Points converging to the period-4 orbit are shown in black. Expansion of the box shown in Fig. 2(a).

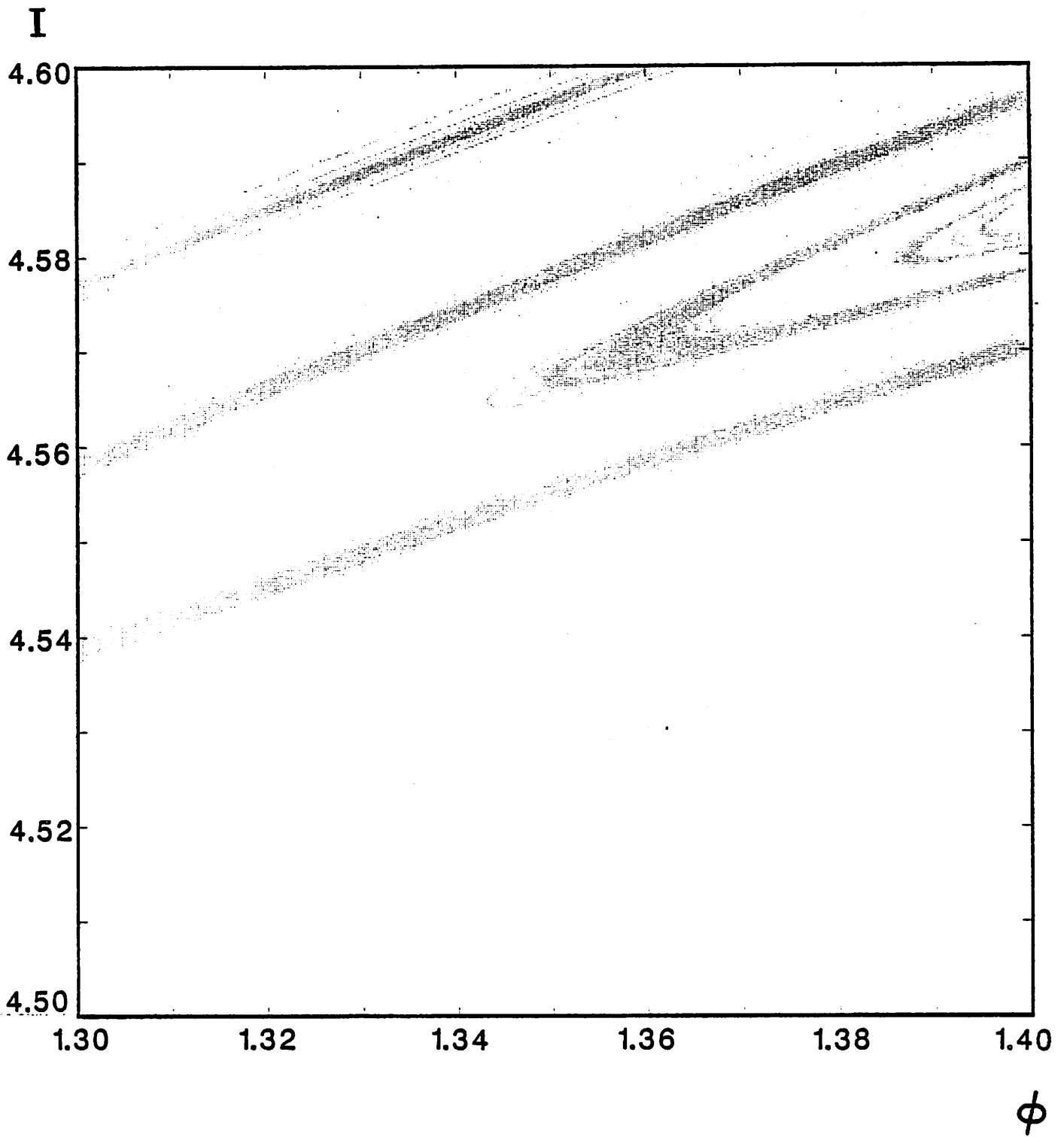


Fig. 2(c). Basin of attraction of the period-4 orbit. Points converging to the period-4 orbit are shown in black. Expansion of the box shown in Fig. 2(b).

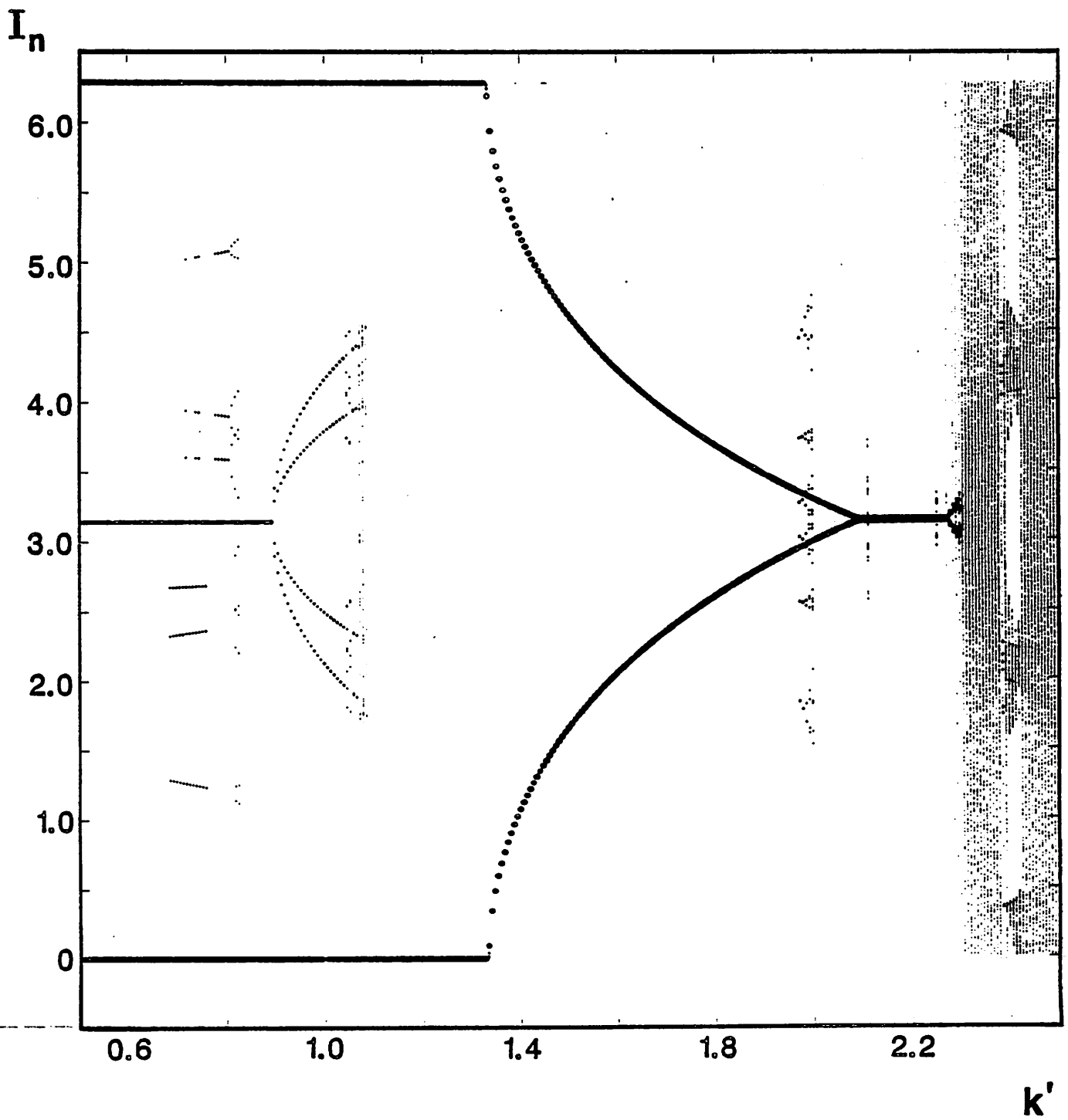


Fig. 3(a). Bifurcation diagrams versus k' for $r = 2.0$. Plotting vertically the I_n state variable.

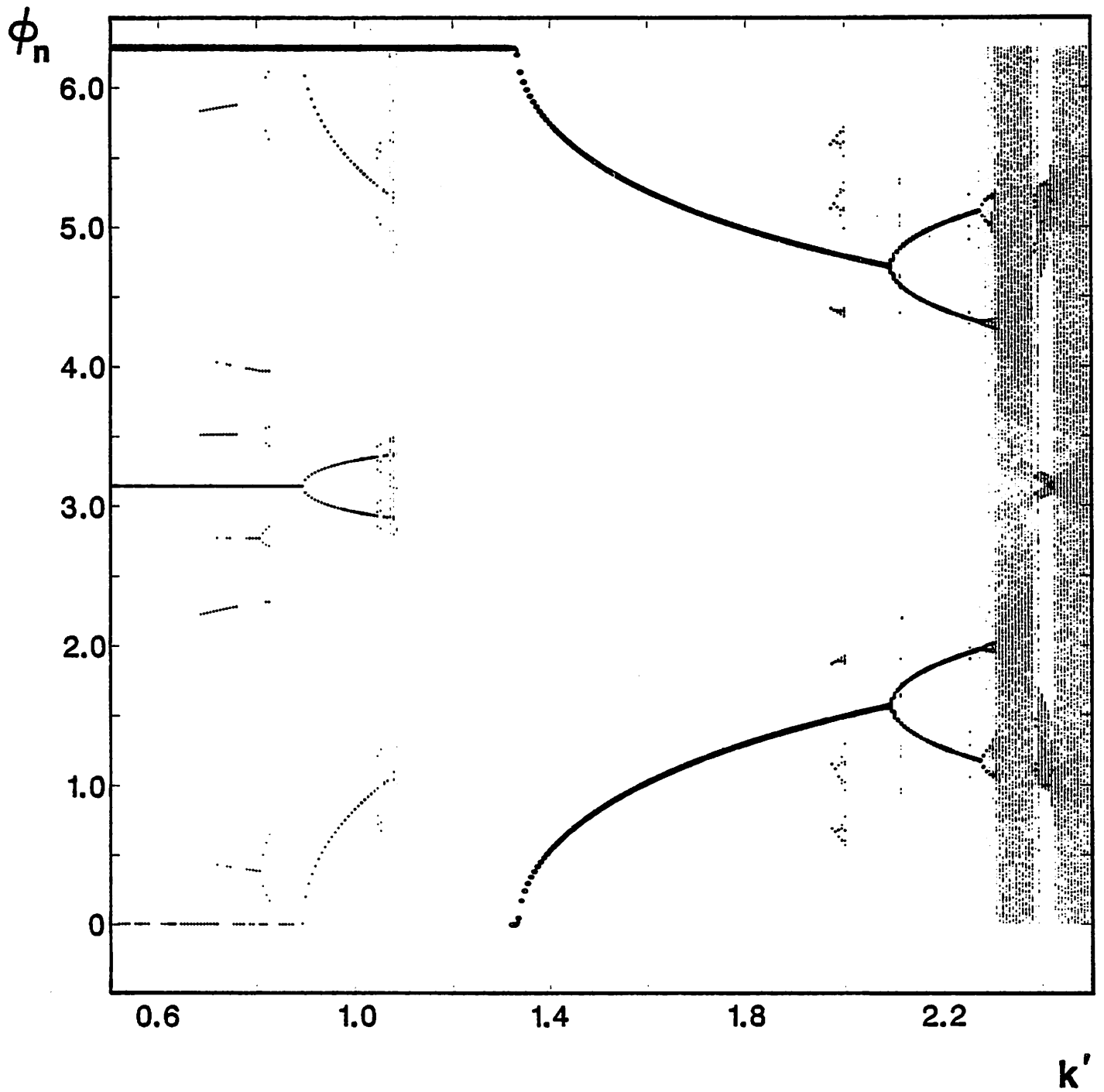


Fig. 3(b). Bifurcation diagrams versus k' for $r = 2.0$. Plotting vertically the ϕ_n state variable.

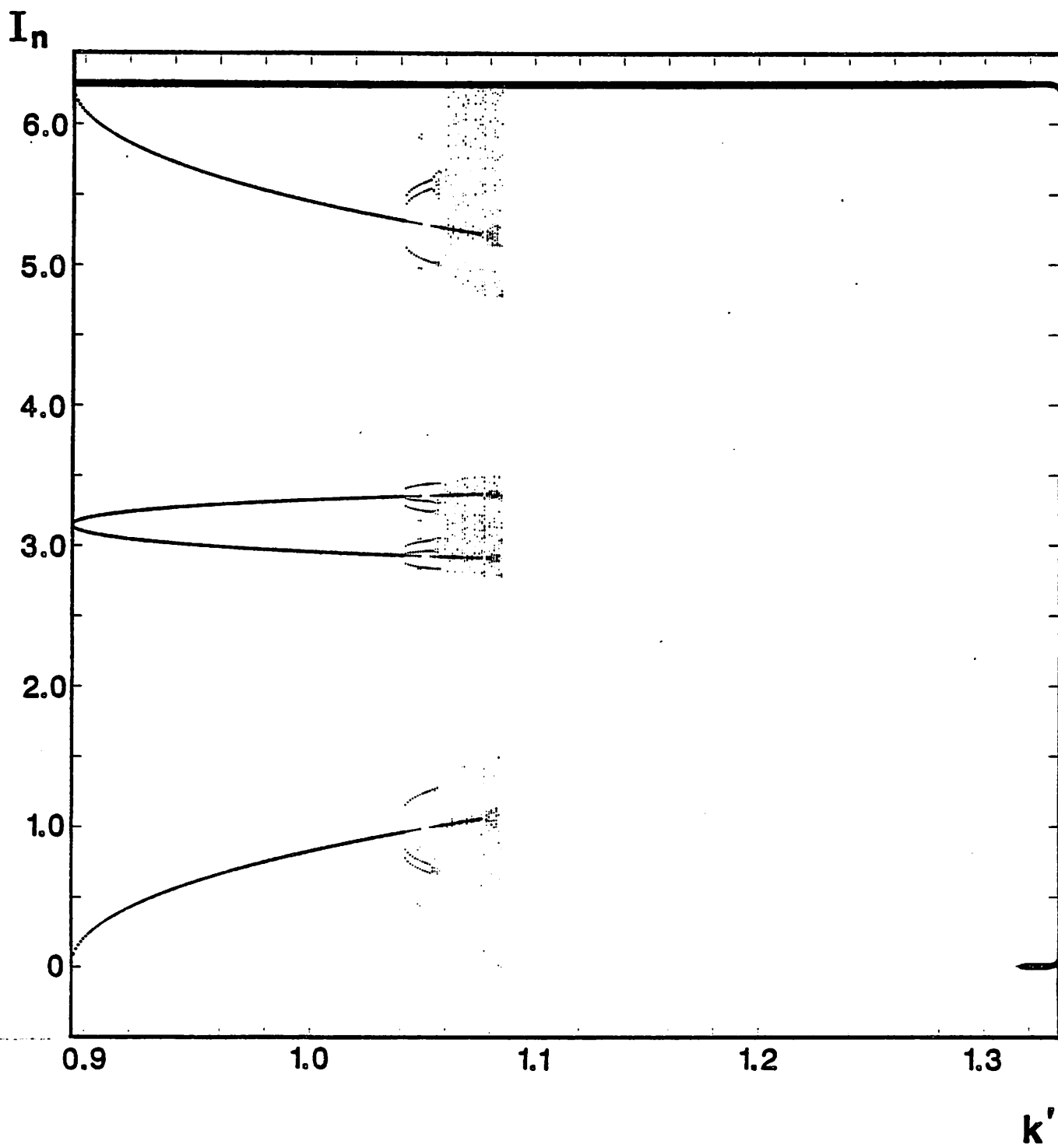


Fig. 4(a). Bifurcation diagrams I versus k' restricted by inequality (12). $r = 2$.

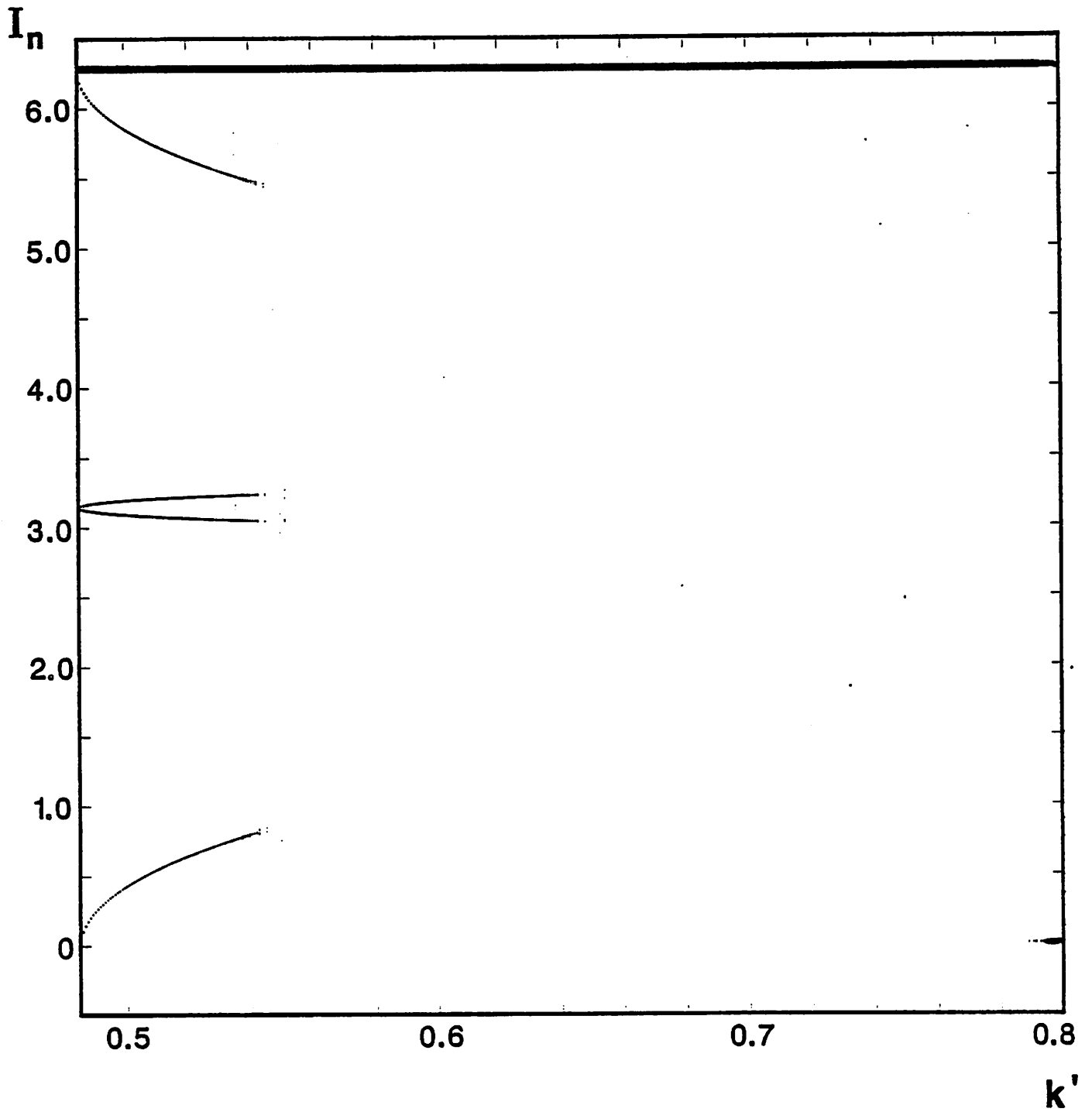


Fig. 4(b). Bifurcation diagrams I versus k' restricted by inequality (12). $r = 4$.

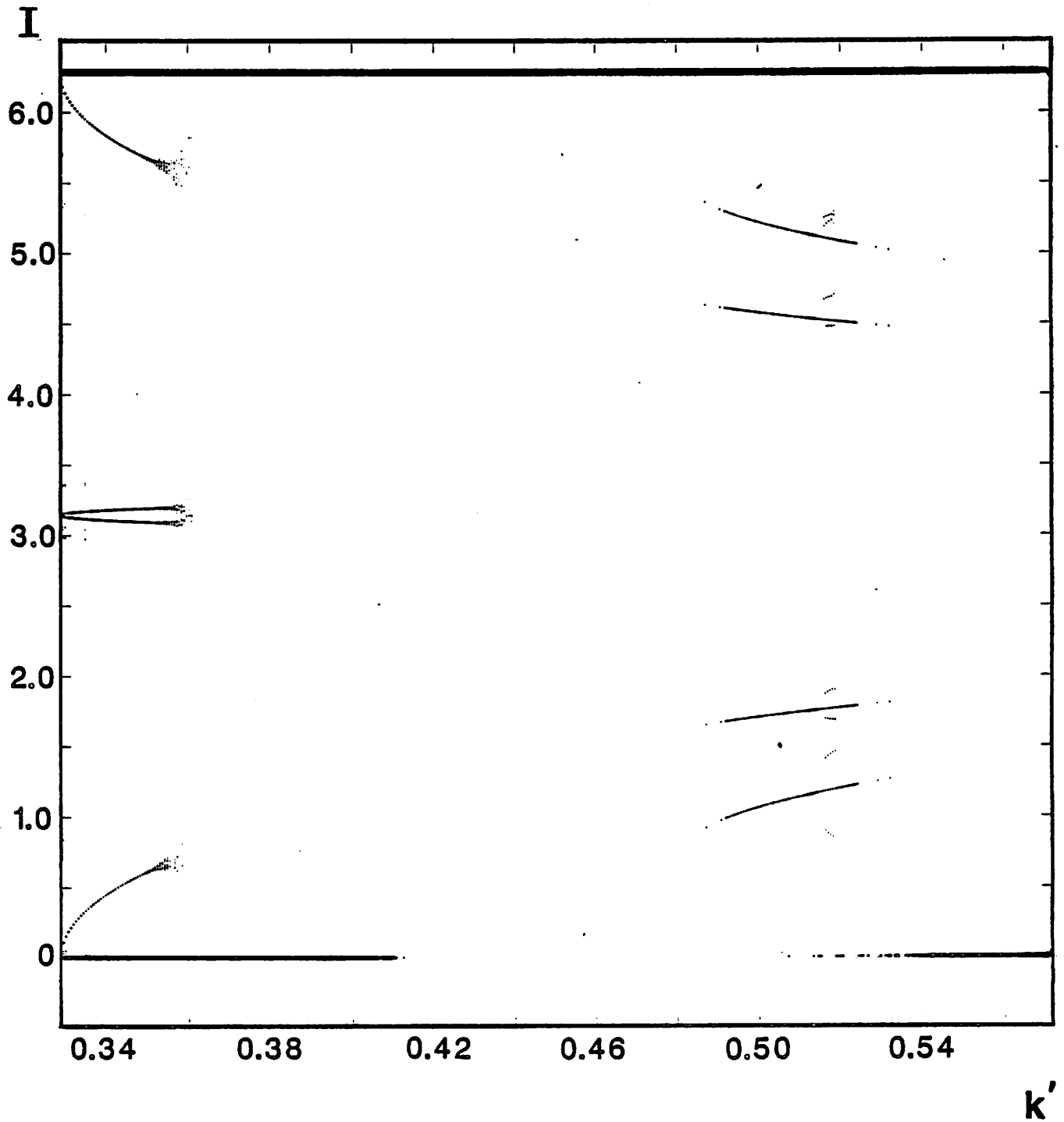


Fig. 4(c). Bifurcation diagrams I versus k' restricted by inequality (12). $r = 6$.

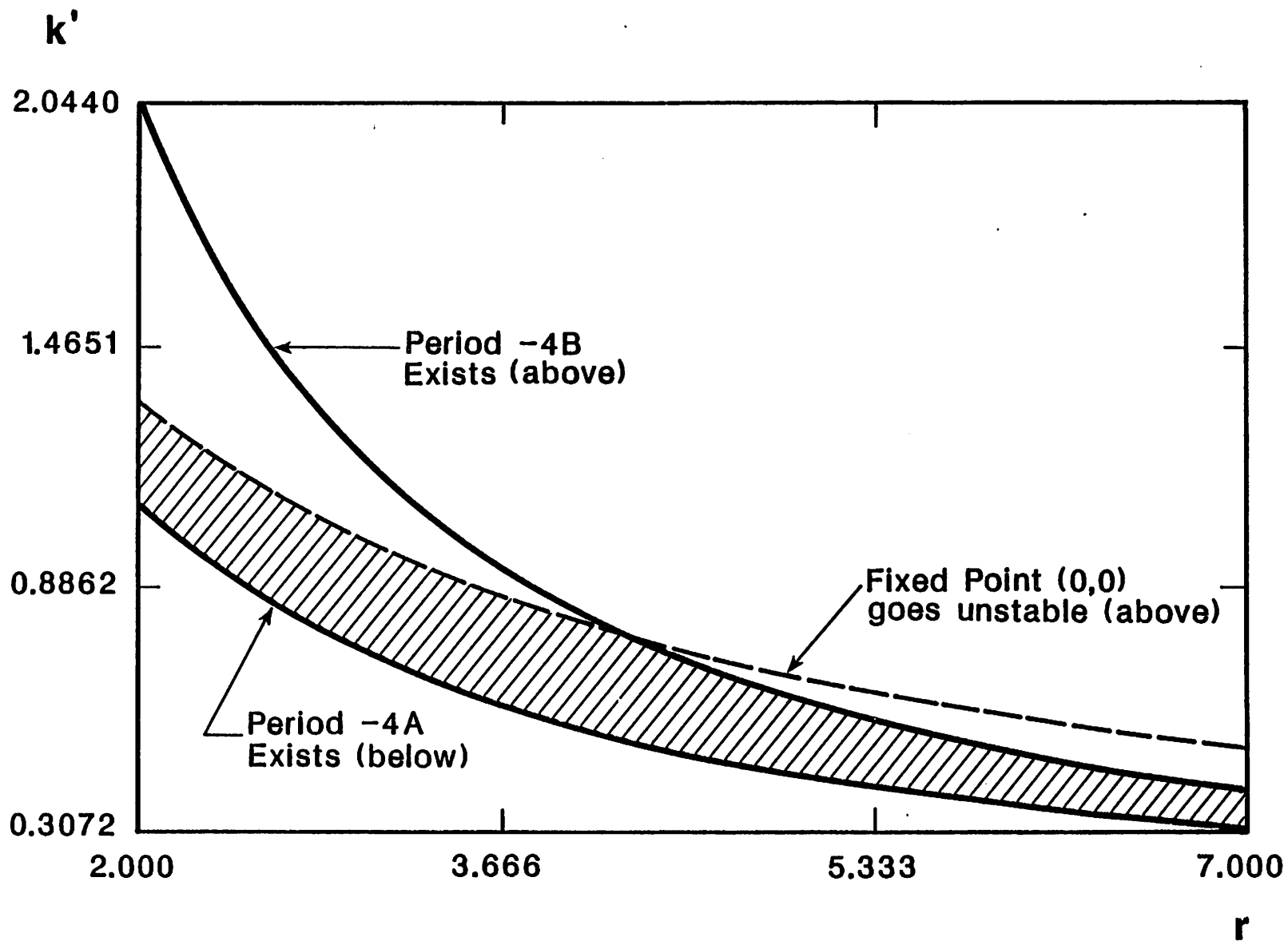


Fig. 5. Boundaries of existence of selected periodic orbits.

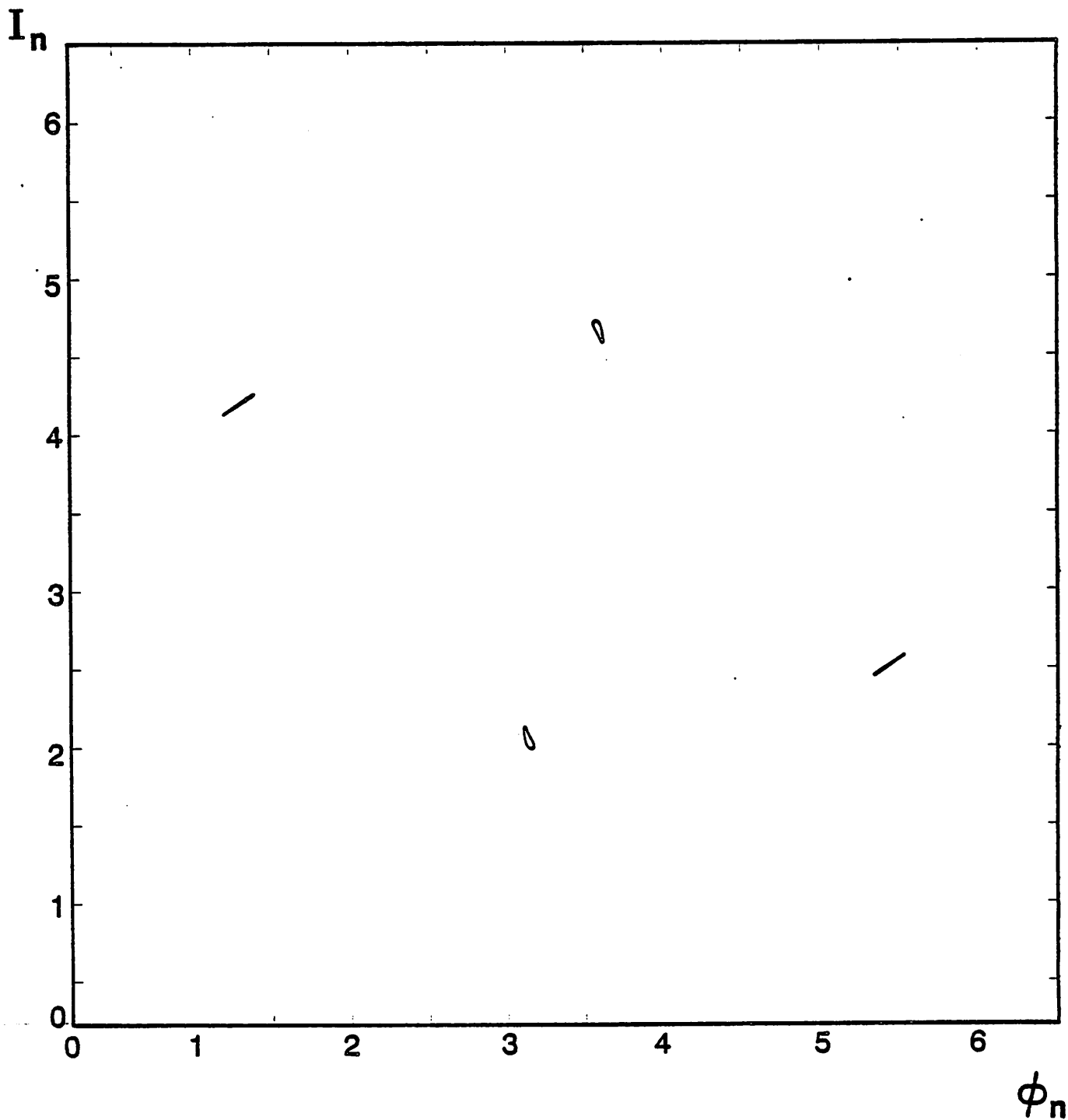


Fig. 6. Almost periodic orbit occurring when $r = 2.0$ and $k' = 1.085$.

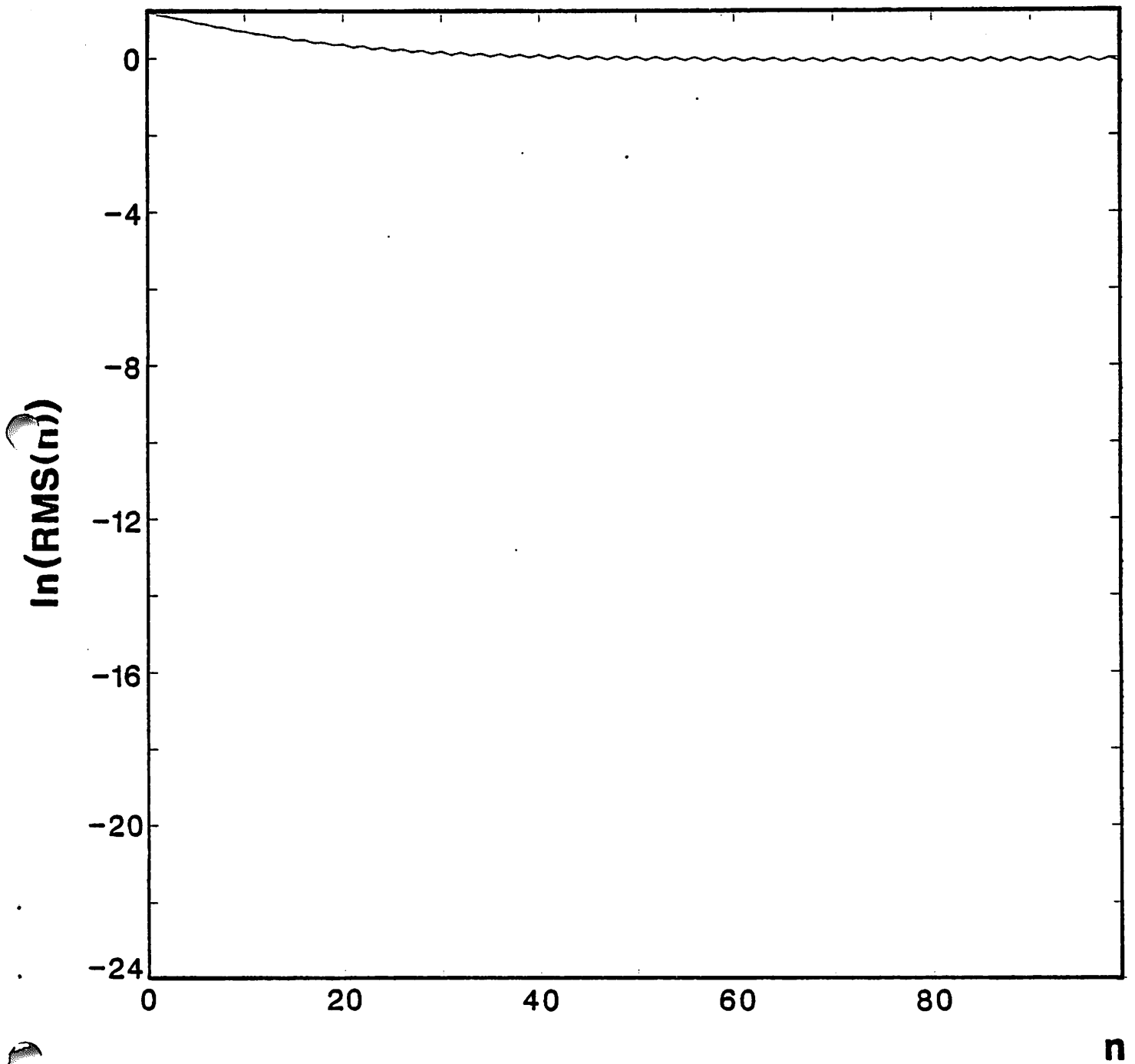


Fig. 7(a). Convergence statistics $\ln RMS$ versus n ; $r = 4$ for all plots. $k' = 0.5400$.

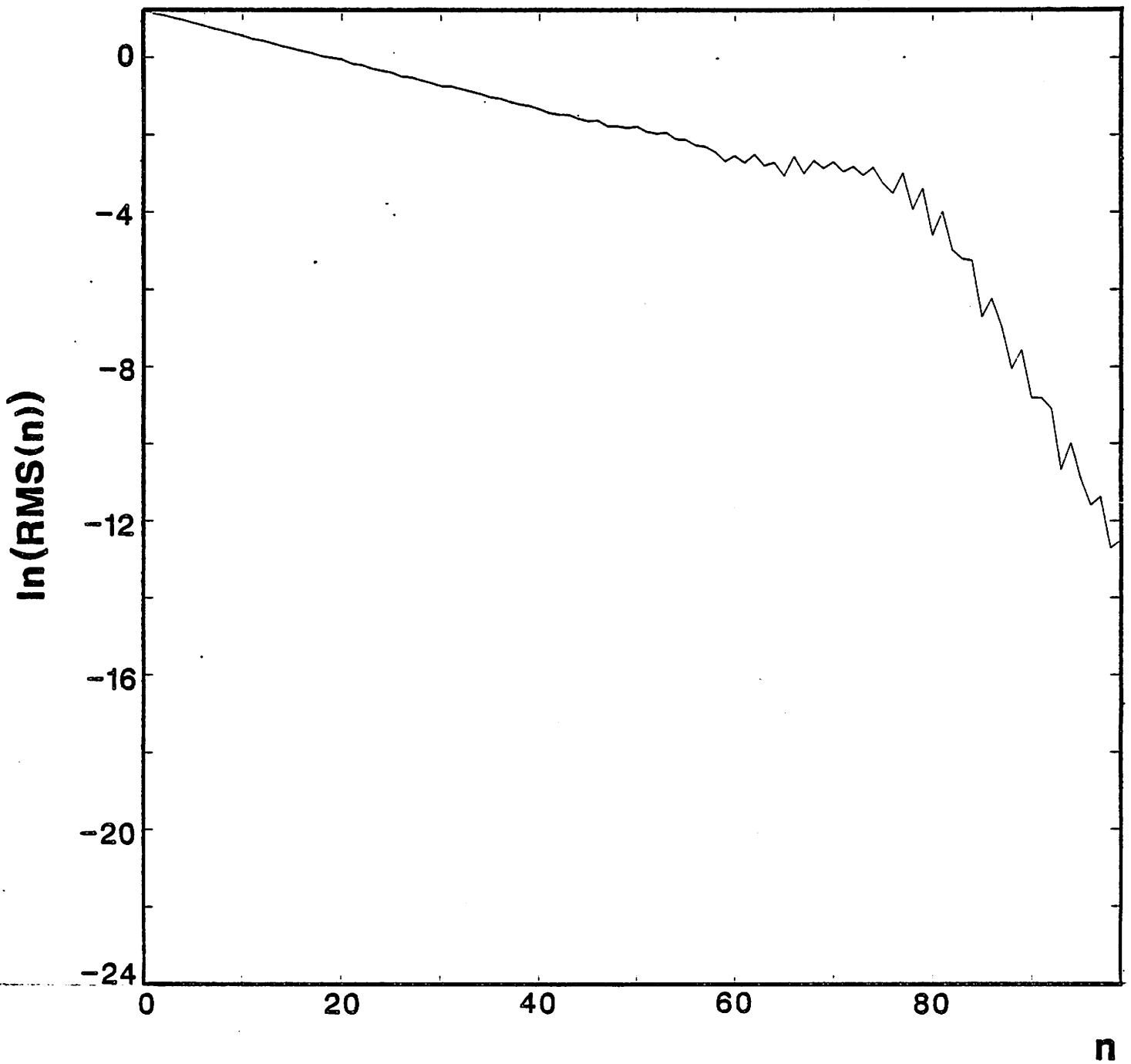


Fig. 7(b). Convergence statistics $\ln RMS$ versus n ; $r = 4$ for all plots. $k' = 0.6143$.

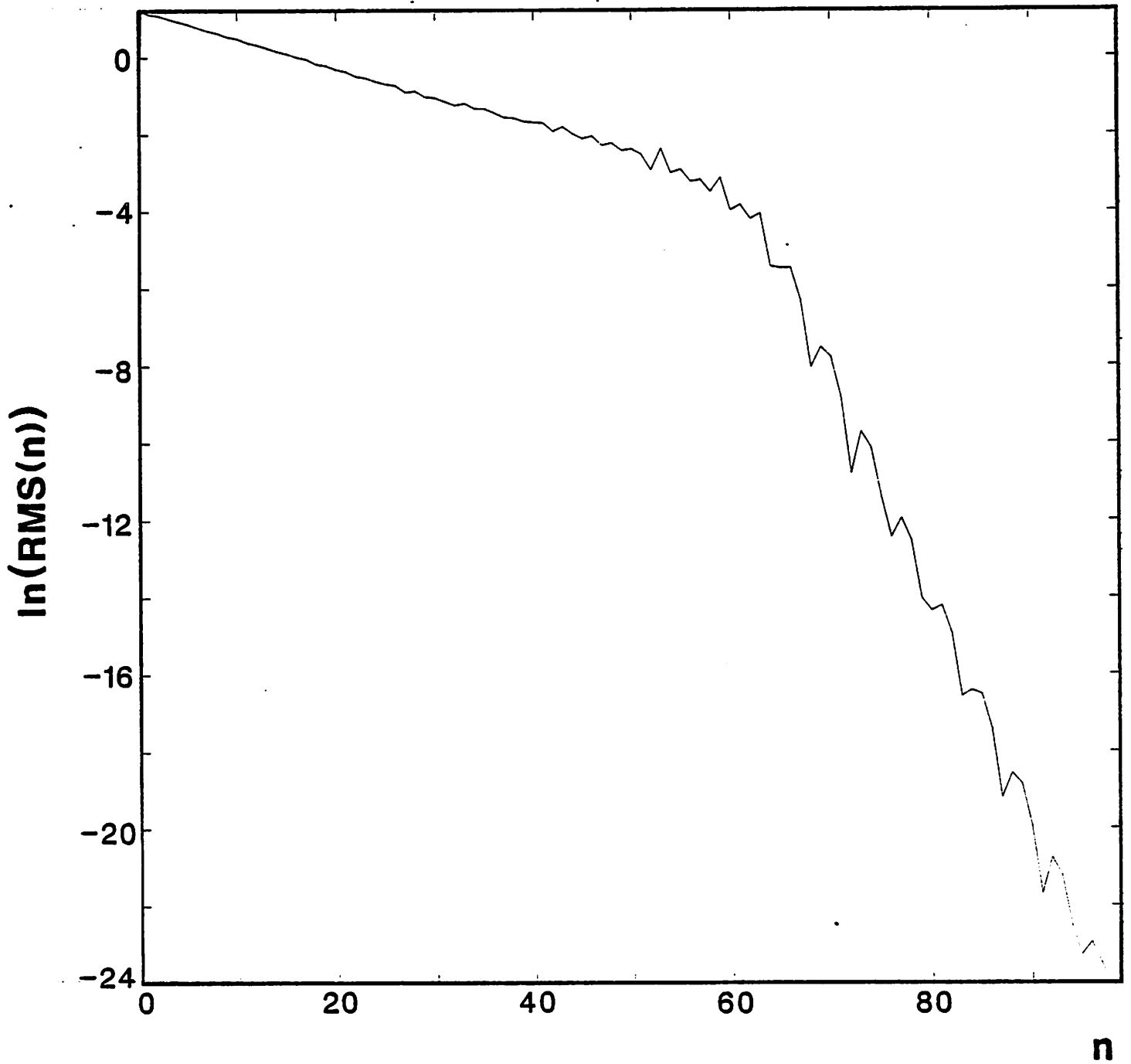


Fig. 7(c). Convergence statistics $\ln \text{RMS}$ versus n ; $r = 4$ for all plots. $k' = 0.6886$.

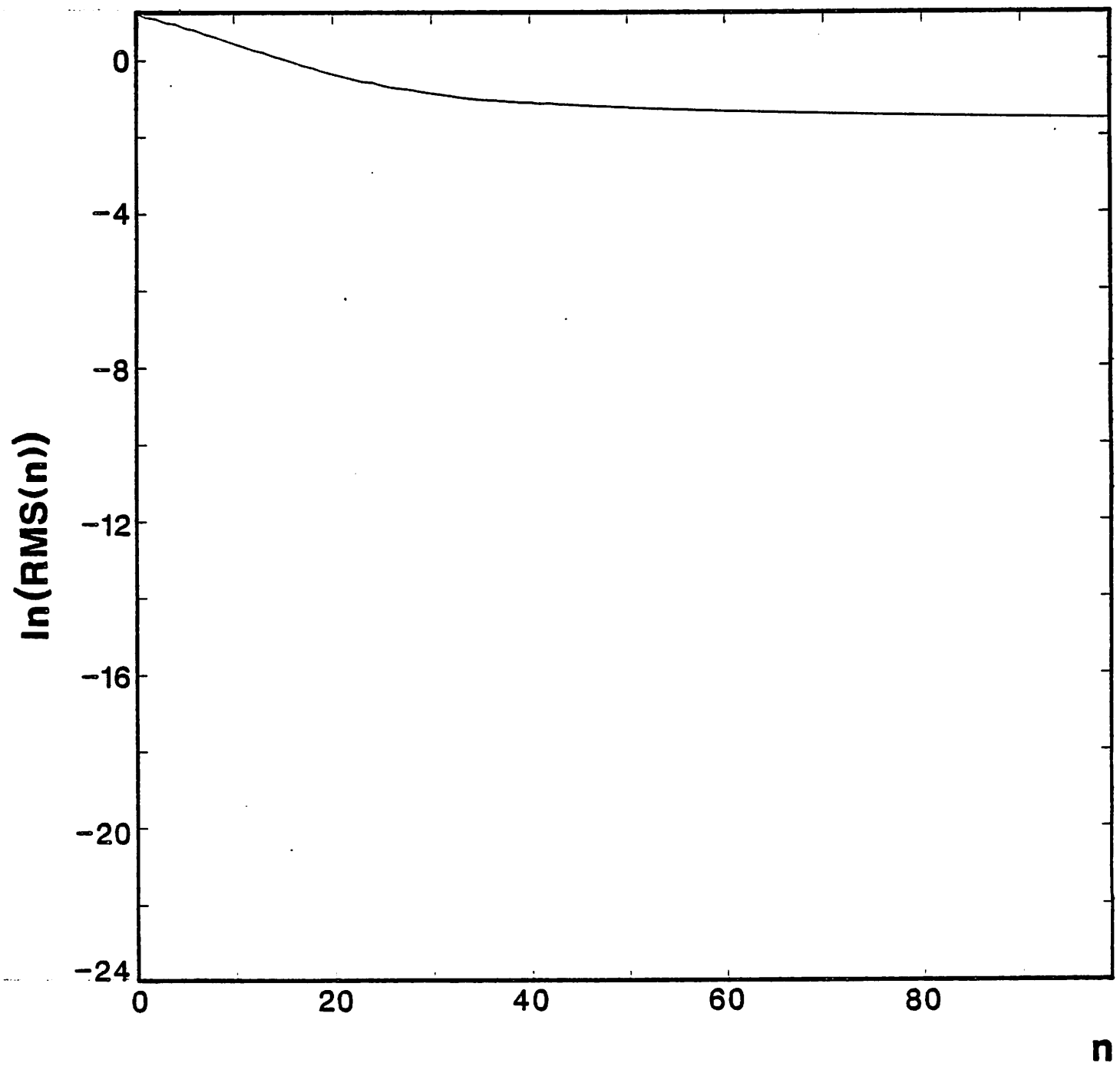


Fig. 7(d). Convergence statistics $\ln RMS$ versus n ; $r = 4$ for all plots. $k' = 0.8000$.

I

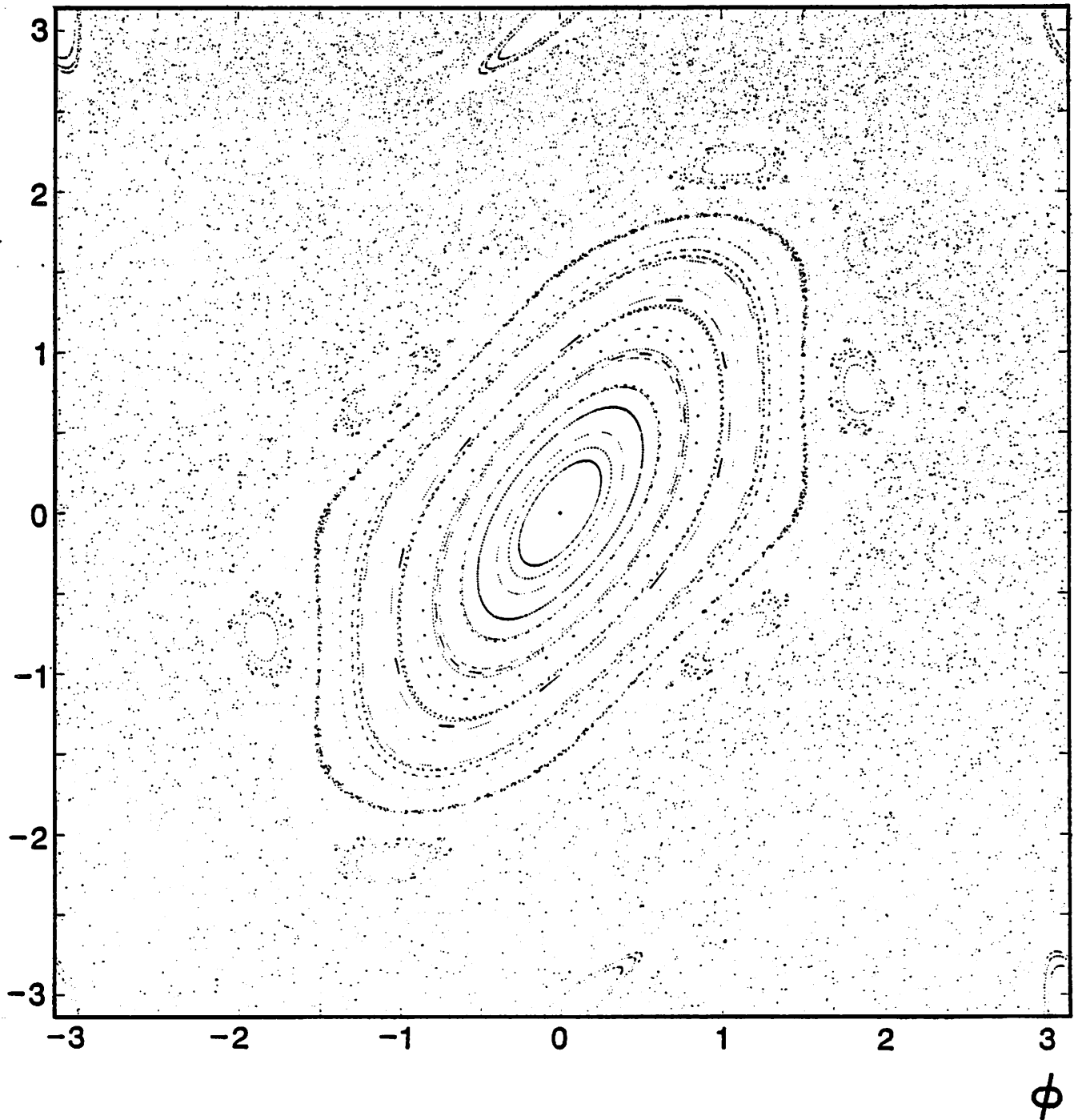


Fig. 8(a). I versus ϕ for the standard map. $K = 1.60$.

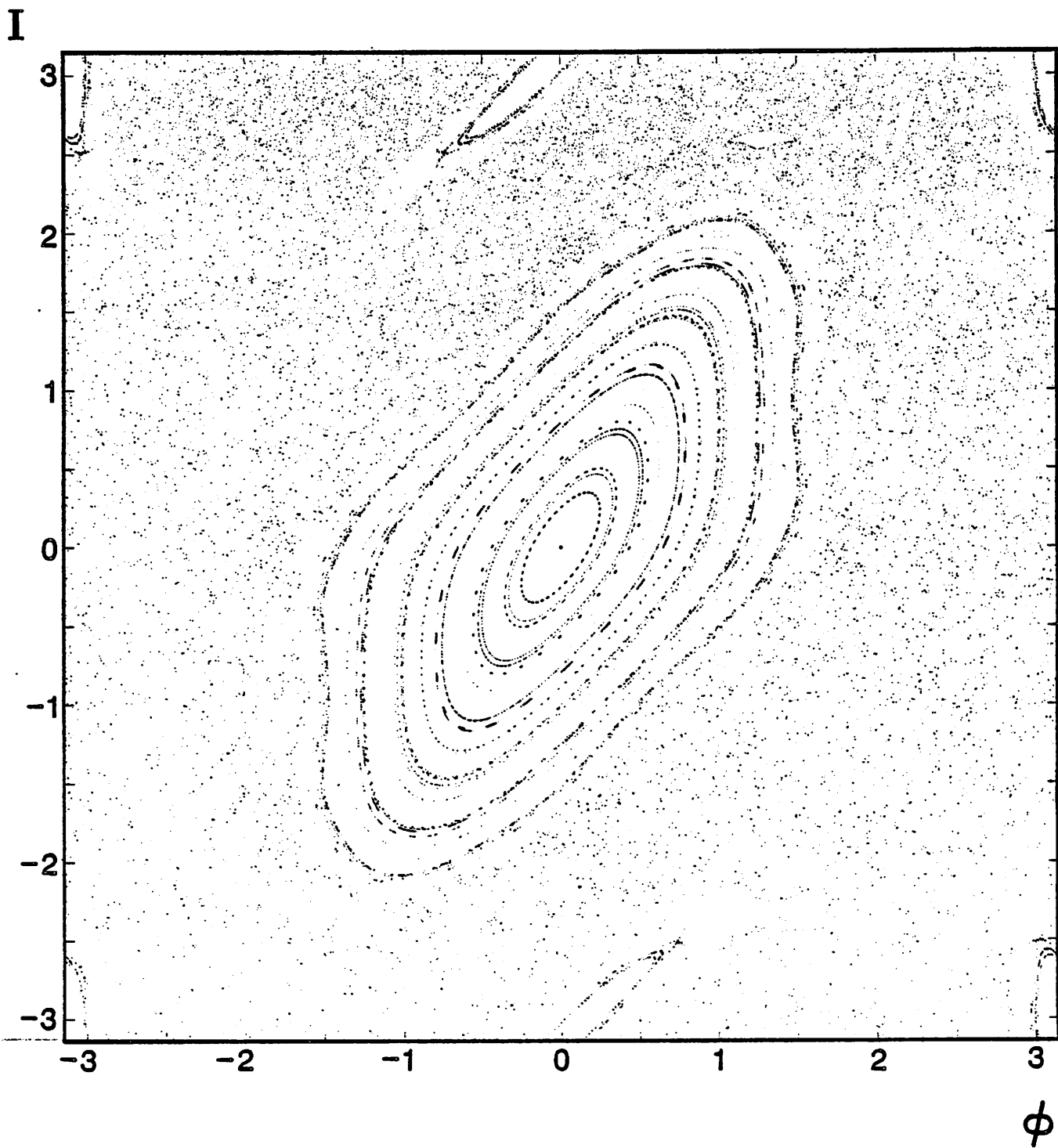


Fig. 8(b). I versus ϕ for the standard map. $K = 1.87$.

I

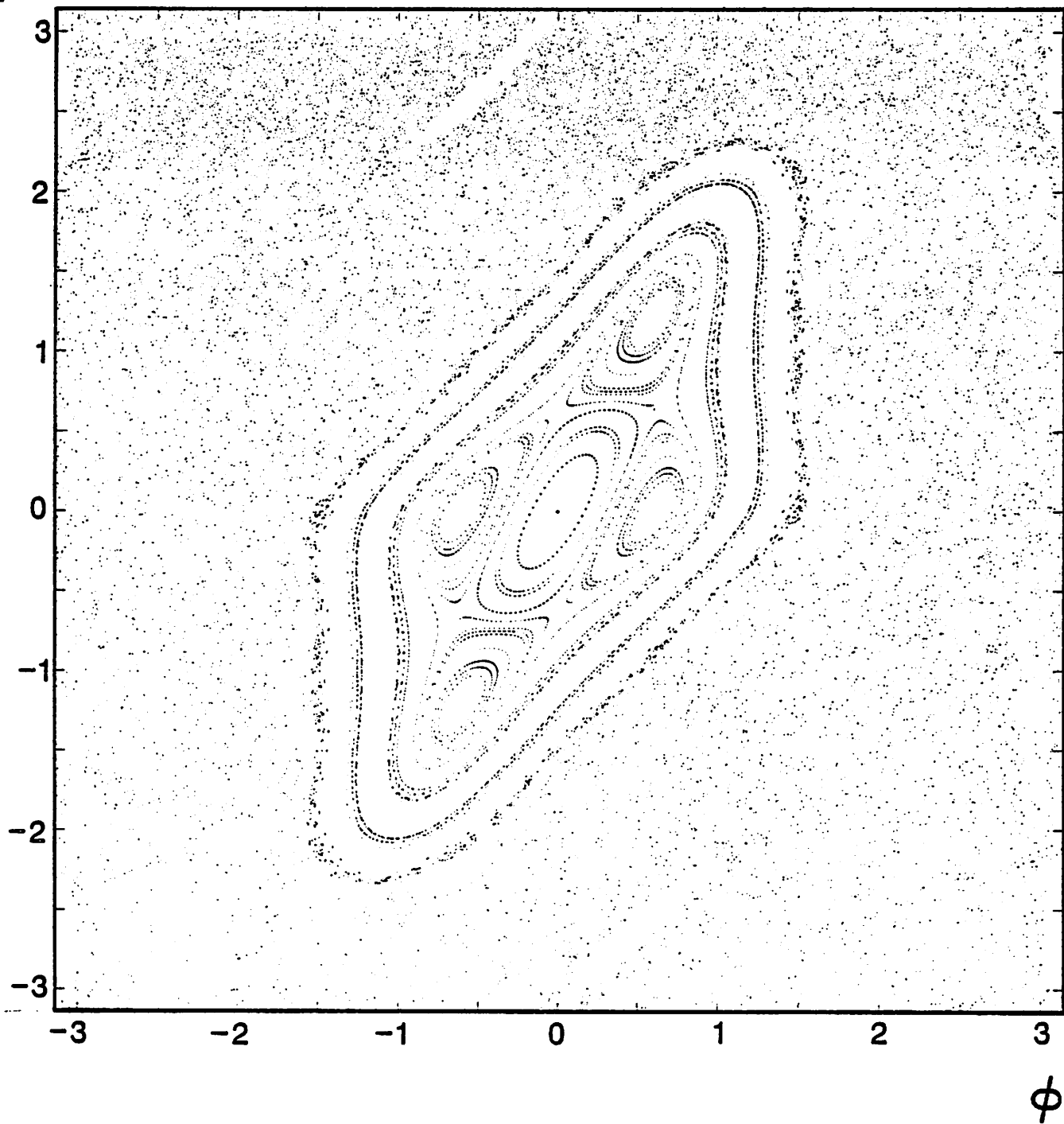


Fig. 8(c). I versus ϕ for the standard map. $K = 2.13$.

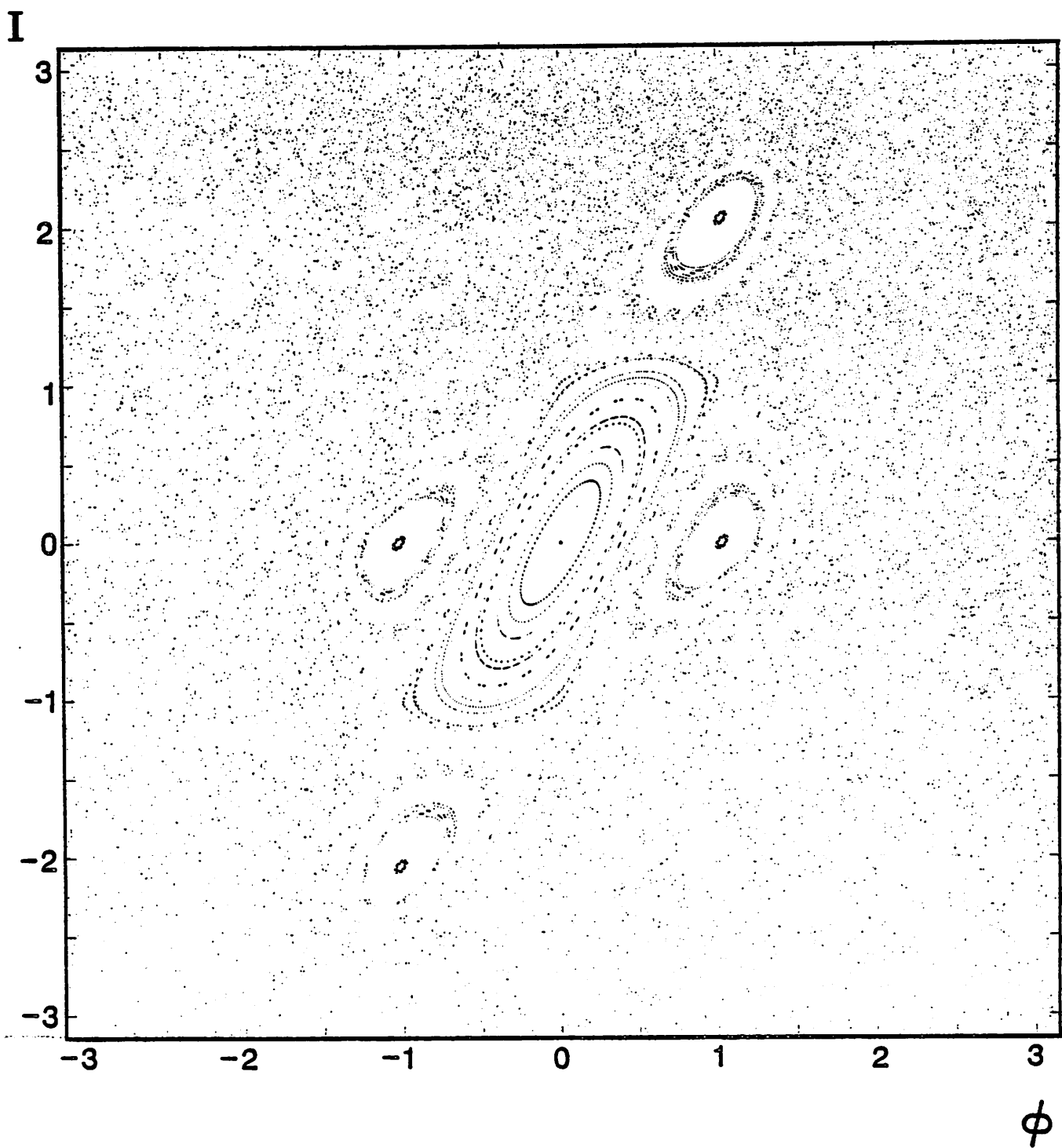


Fig. 8(d). I versus ϕ for the standard map. $K = 2.40$.